

Research Paper

ROS-Responsive Activatable Photosensitizing Agent for Imaging and Photodynamic Therapy of Activated Macrophages

Hyunjin Kim¹, Youngmi Kim², In-Hoo Kim¹, Kyungtae Kim³✉ and Yongdoo Choi¹✉

1. Molecular Imaging & Therapy Branch, Division of Convergence Technology, National Cancer Center, 111 Jungbalsan-ro, Ilsandong-gu, Gyeonggi-do 410-769, Republic of Korea;
2. Department of Chemistry, Institute of Nanosensor and Biotechnology, Dankook University, 126 Jukjeon-dong, Yongin-si, Gyeonggi-do 448-701, Republic of Korea;
3. Molecular Epidemiology Branch, Division of Cancer Epidemiology and Prevention, National Cancer Center, 111 Jungbalsan-ro, Ilsandong-gu, Gyeonggi-do 410-769, Republic of Korea.

✉ Corresponding author: Yongdoo Choi, Ph.D. Tel: +82-31-920-2512 E-mail: ydchoi@ncc.re.kr Or Kyungtae Kim, Ph.D. Tel: +82-31-920-2557 E-mail: bioktkim@ncc.re.kr.

© Ivyspring International Publisher. This is an open-access article distributed under the terms of the Creative Commons License (<http://creativecommons.org/licenses/by-nc-nd/3.0/>). Reproduction is permitted for personal, noncommercial use, provided that the article is in whole, unmodified, and properly cited.

Received: 2013.07.05; Accepted: 2013.09.25; Published: 2013.12.01

Abstract

The optical properties of macrophage-targeted theranostic nanoparticles (MacTNP) prepared from a Chlorin e6 (Ce6)-hyaluronic acid (HA) conjugate can be activated by reactive oxygen species (ROS) in macrophage cells. MacTNP are nonfluorescent and nonphototoxic in their native state. However, when treated with ROS, especially peroxyxynitrite, they become highly fluorescent and phototoxic. *In vitro* cell studies show that MacTNP emit near-infrared (NIR) fluorescence inside activated macrophages. The NIR fluorescence is quenched in the extracellular environment. MacTNP are nontoxic in macrophages up to a Ce6 concentration of 10 μ M in the absence of light. However, MacTNP become phototoxic upon illumination in a light dose-dependent manner. In particular, significantly higher phototoxic effect is observed in the activated macrophage cells compared to human dermal fibroblasts and non-activated macrophages. The ROS-responsive MacTNP, with their high target-to-background ratio, may have a significant potential in selective NIR fluorescence imaging and in subsequent photodynamic therapy of atherosclerosis with minimum side effects.

Key words: Reactive oxygen species, macrophage, theranostics, activatable, photodynamic therapy.

Introduction

Rupture of atherosclerotic plaques and the associated thrombotic complications such as myocardial infarction, stroke, and limb ischemia remains the leading cause of cardiovascular-related mortality worldwide [1-3]. Macrophages, constituting up to 20% of the cells within atherosclerotic lesions, are known to play a key role both in the development of atherosclerosis and in the formation of unstable plaques vulnerable to rupture [4]. Therefore, a large

number of active macrophages in plaques have been considered a biomarker for plaque instability [5] and a prime target for the imaging and therapy of atherosclerosis [6, 7]. However, it is obvious that only the plaque-associated macrophages are undesirable, while the majority of monocytes/macrophages in circulation and in healthy tissues play important roles for homeostasis and immunity. Therefore, a method to selectively detect and kill only those macrophages

in the plaque would be desirable.

Photodynamic therapy (PDT) using a combination of chemical photosensitizers, light, and molecular oxygen has long been used to successfully treat cancers [8]. Photosensitizers are typically nontoxic to cells in the absence of light, but become highly cytotoxic when the molecules accumulated at target sites are excited by light radiation of a specific wavelength. *In vivo* studies have shown that PDT promotes the stabilization of atherosclerotic plaques and inhibits plaque progression by reducing the macrophage content [9-11]. Even though a number of photosensitizers were shown to accumulate preferentially in atherosclerotic plaques, the systemic administration of most photosensitizing agents leads to significant side effects (i.e., prolonged skin photosensitivity) due to nonspecific localization of the hydrophobic photosensitizers within the skin [12-15]. Therefore, various types of macrophage-targeting PDT agents and multifunctional theranostics have been tested to improve the efficacy of PDT and the selective imaging of the activated macrophages [16-20]. An ongoing challenge in imaging and atherosclerosis therapy involves the use of “activatable” PDT agents that have shown great potential against cancers [21-30]. Activatable PDT agents with controlled optical properties are nonfluorescent and nonphototoxic in their native states, but become highly fluorescent and phototoxic upon exposure to various stimuli at target sites (i.e., enzymes and low pH). These activatable PDT agents were shown to be highly efficient in selectively killing target cancer cells while minimizing unwanted skin photosensitivity. Recently, we showed the first successful *in vivo* results demonstrating the potential utility of an enzyme-activatable PDT agent in near-infrared (NIR) fluorescence imaging and the

subsequent PDT of atherosclerosis [31]. The cathepsin B-activatable photodynamic theranostic agent reduced cathepsin-B activity in mouse atheromata and stabilized inflammatory plaques by selectively killing the activated macrophages in the diseased regions.

This study aims to develop a reactive oxygen species (ROS)-responsive PDT agent as a new theranostic agent for targeted imaging and therapy of the atherosclerotic lesions. It is well known that ROS generated in activated macrophages play an important immune role [32, 33]. Importantly, excess ROS are produced by activated macrophage cells in various pathogenic conditions, including atherosclerosis [34, 35]. Therefore, we assumed that the excess ROS might represent a good target for developing macrophage-targeted “activatable” theranostics. According to previous reports, polysaccharides including hyaluronic acid could be depolymerized by ROS [36, 37]. Therefore, we prepared macrophage-targeted theranostic nanoparticles (MacTNP) by conjugating photosensitizers to hyaluronic acid (Figure 1 and 2). We expected that fluorescence and singlet oxygen generated from the MacTNPs in the native state would be inhibited due to self-quenching effect between the conjugated photosensitizers. When MacTNPs are internalized by the activated macrophages, the excess ROS in the cells degrades the nanoparticles by cleaving the chemical bonds of hyaluronic acid. This results in photosensitizer release from the nanoparticles, which results in fluorescence emission and singlet oxygen generation. Such a ROS-responsive MacTNP may have great potential in selective NIR fluorescence imaging with high target-to-background ratio and subsequent PDT of atherosclerosis with minimized side effects (i.e., skin photosensitivity).

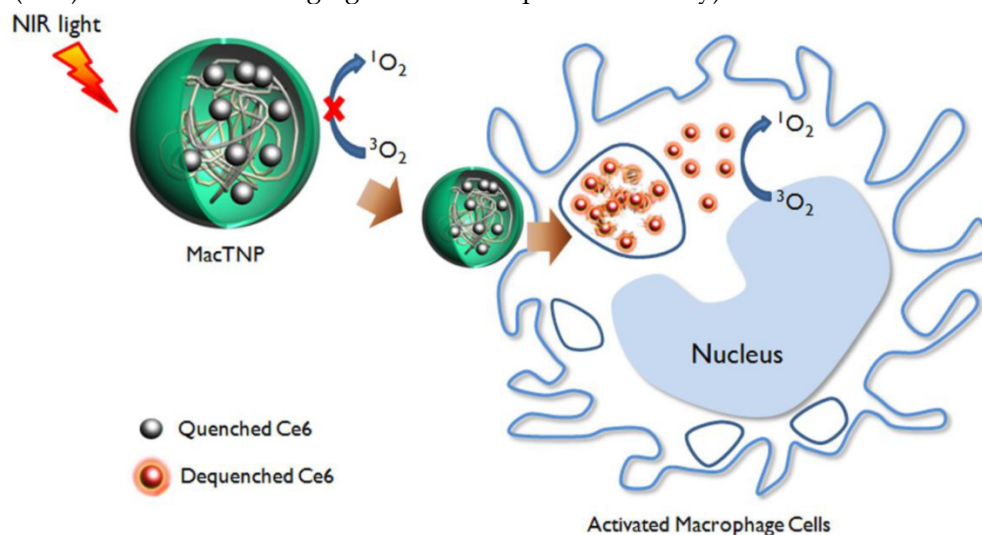


Fig 1. A schematic illustration of activatable nano-photomedicine for macrophage-targeted fluorescence imaging and subsequent photodynamic therapy. Fluorescence and singlet oxygen generation of MacTNP are quenched in the native state. When ROS inside the activated macrophage cells degrade MacTNP, the photosensitizers (Ce6s) are de-quenched and become highly fluorescent and phototoxic.

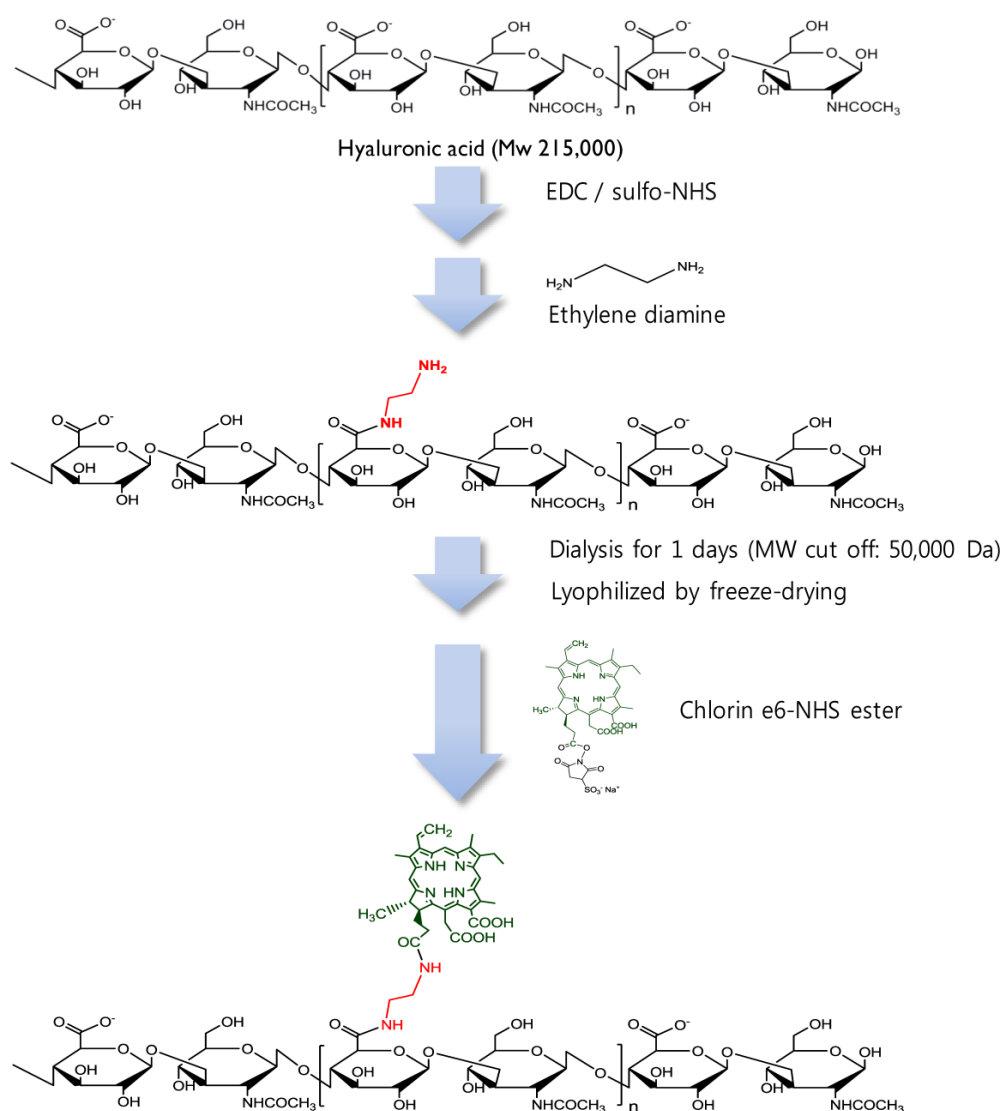


Fig 2. Synthetic production of HA-Ce6 conjugates.

Materials and Methods

Materials

Hyaluronic acid (HA, MW 215,000 Da) was purchased from Lifecore Biomedical (Chaska, MN, USA). 1-Ethyl-3-(3-dimethylaminopropyl) carbodiimide (EDC), sulfo-N-hydroxysulfosuccinimide (sulfo-NHS), ethylene diamine, and hyaluronidase (HAase, 1,228 units/mg) were purchased from Sigma-Aldrich (MO, USA). Chlorin e6 (Ce6) and dialysis membranes (MW cut-off: 50,000 Da) were purchased from Frontier Scientific (UT, USA) and Spectrum Laboratories (CA, USA), respectively. Singlet Oxygen Sensor Green (SOSG), which is a singlet-oxygen-detecting reagent, was obtained from Invitrogen (NY, USA).

Lipopolysaccharide (LPS) and recombinant murine interferon-gamma (INF- γ) were purchased from

List Biological Laboratories, INC. (CA, USA) and PeroTech (NJ, USA), respectively. The Raw 264.7 macrophage cell line was obtained from the American Type Culture Collection (Rockville, MD, USA). Human dermal fibroblast (HDF) cells were kindly provided by Dr. Sang Chul Park (College of Medicine, Seoul National University, Republic of Korea). Both cell lines were maintained in Dulbecco's Modified Eagle Medium (DMEM; GIBCO[®], Invitrogen) supplemented with 10% (v/v) fetal bovine serum (FBS) and 1% antibiotic-antimycotic solution in a humidified incubator at 37°C, 5% CO₂.

Preparation of MacTNP

MacTNP were prepared from a hyaluronic acid-chlorin e6 (HA-Ce6) conjugate (Figure 2). First, amine-functionalized HA was synthesized by conjugating ethylene diamine with the carboxylic acid component of HA using standard EDC/NHS chem-

istry. Briefly, 200 mg of HA was dissolved in phosphate buffer solution (pH 7.4, 10 mM, 19 mL); EDC (35 mM, 0.5 mL) and sulfo-NHS (42 mM, 0.5 mL) were sequentially added to the HA-dissolved aqueous solution. After 30 min, ethylene diamine (93 mg), dissolved in the phosphate buffer (pH 7.4, 10 mM, 1 mL) was added to the activated HA solution, and the reaction was allowed to proceed overnight at room temperature. The reactant was then dialyzed against deionized (DI) water and lyophilized. To conjugate the amine-functionalized HA with Ce6, the carboxylic acid of Ce6 (50 mg, 10 mL) was activated with EDC (21 mM) and sulfo-NHS (28 mM) in dimethyl sulfoxide (DMSO). Aminated HA (200 mg) was dissolved in dimethylformamide (DMF):H₂O cosolvent (1:1 v/v, 5 mL), mixed with the activated Ce6 solution, and then reacted for 18 h at room temperature. The resulting HA-Ce6 solution was dialyzed against phosphate buffer (pH 7.4, 10 mM) and then with DI water to remove unreacted Ce6s and the byproducts. Self-assembled HA-Ce6 nanoparticles (henceforth called MacTNP) were formed during the dialysis procedure in the aqueous solution. MacTNP was finally freeze-dried. The products obtained at each step were analyzed by proton nuclear magnetic resonance (¹H-NMR) (Supplementary Material: Figure S1).

Characterization of MacTNP

The surface charge of MacTNP was measured using a zeta potential/particle-sizer (Malvern Instrument, Malvern, UK), after dispersing the particles in DI water. The hydrodynamic size was measured after dispersing in phosphate-buffered saline (PBS; 6.7 mM, pH 7.4, 154 mM NaCl).

For the analysis of the optical properties, MacTNP were dispersed in PBS. For comparison, free Ce6 was dissolved in Tween 20-containing PBS solution (1% v/v) to avoid photosensitizer aggregation in the aqueous solution. Then UV/Vis spectra of MacTNP and free Ce6 solutions were measured with an UV/Vis spectrometer (DU730, Beckman Coulter, Brea, CA) to check the aggregation of Ce6s in the nanoparticles (final concentration, 5 μM Ce6). The concentration of Ce6 in MacTNP and free Ce6 stock solutions was calculated by dissolving the nanoparticles in 0.1 M NaOH/0.1% sodium dodecyl sulfate (SDS), and then the absorbance at 400 nm was measured. Ce6 is known to have a molar extinction coefficient of $1.5 \times 10^5 \text{ M}^{-1} \text{ cm}^{-1}$ at 400 nm [38]. The fluorescence spectra of MacTNP and free Ce6 (with 400 nm excitation) were obtained on a multifunctional microplate reader (Safire 2; Tecan, Männedorf, Switzerland). MacTNP and free Ce6 were maintained at a final concentration of 5 μM Ce6.

The inhibitory characteristics of singlet oxygen

generation (SOG) in MacTNP were evaluated by measuring the fluorescence intensity increase of SOSG during light irradiation, which was then compared with that of free Ce6. SOSG was dissolved in PBS saturated with oxygen gas containing either MacTNP or free Ce6. The final concentration of SOSG reagent was maintained at 1 μM. The final concentration of MacTNP and free Ce6 were 0.5 μM Ce6. SOSG fluorescence intensity (λ_{ex} 504 nm, λ_{em} 525nm) was then measured periodically, during light irradiation with a 670-nm CW laser (irradiation dose rate 50 mW/cm²).

ROS-responsive recovery of fluorescence and SOG in the MacTNP

To examine the ROS-mediated recovery of fluorescence and SOG, MacTNP were reacted with various ROS and the fluorescence intensity and SOG were measured. ROS generators were prepared according to a previous report [37]: 50 μM KO₂ for the superoxide anion (O₂^{•-}), 50 μM H₂O₂ with 5 μM ferrous perchlorate for the hydroxyl radical (•OH), 50 μM hydrogen peroxide (H₂O₂) with 50 μM NaOCl for hypochlorite (OCl⁻), and 50 μM H₂O₂ with 10 μM nitrite for peroxyxynitrite (ONOO⁻) [37]. MacTNP (final concentration: 0.5 μM Ce6) were incubated for 2 h with various ROS in PBS (pH 7.4), and then the fluorescence intensity of Ce6 was measured (λ_{ex} 400 nm, λ_{em} 660 nm). Next, the samples were mixed with an oxygen-saturated PBS solution containing concentrated SOSG. The final concentration of SOSG was adjusted to 1 μM. The fluorescence intensities of the samples were measured before light irradiation to check if ROS in the samples could alter the fluorescence of SOSG. Finally, SOSG fluorescence changes were measured after irradiating the solutions with a 670-nm continuous wave (CW) laser (irradiation dose rate 50 mW/cm²) for 120 s. All the experiments were performed in quadruplicate.

In another set of experiments, the effect of peroxyxynitrite concentration on fluorescence intensity of MacTNP was tested by incubating MacTNP (equiv. Ce6 concentration of 0.5 μM) with peroxyxynitrite at different concentrations (0, 5, 10, 20, 40, and 100 μM) in PBS (pH 7.4) for 2 h, and then measuring the fluorescence intensity of MacTNP (λ_{ex} 400 nm, λ_{em} 660 nm).

All the experiments were performed in quadruplicate.

The effect of hyaluronidase on fluorescence recovery of MacTNP

The effect of hyaluronidase (HAase) on the recovery of MacTNP fluorescence was evaluated by treating MacTNP (equiv. Ce6 concentration of 1 μM) with hyaluronidase in different concentrations (0, 10,

50, 100, and 500 U/mL) in sodium acetate buffer (100 mM, pH 4.5, 100 mM NaCl) for 1 h. Then the samples were diluted with PBS (pH 7.4), and fluorescence intensity of Ce6 was measured (λ_{ex} 400 nm, λ_{em} 660 nm). The experiments were performed in quadruplicate.

Evaluation of fluorescence quenching and recovery in activated macrophage cells: live cell fluorescence imaging

MacTNP and free Ce6 were diluted in fresh DMEM medium supplemented with 10% FBS to obtain 1 μM Ce6.

Raw 264.7 cells were plated at a density of 1×10^6 cells/well in a 12-well plate (BD Biosciences) and incubated for 24 h to allow cell attachment. The cells were activated by treatment with 1 $\mu\text{g}/\text{mL}$ lipopolysaccharide (LPS) and 50 ng/mL interferon-gamma (INF- γ) for 24 h. The cell culture medium was replaced with fresh medium containing the photosensitizers. Then, without washing the cells, NIR fluorescence images (λ_{ex} 640 \pm 15 nm, λ_{em} 690 \pm 25 nm) of the activated macrophage cells were recorded every 15 min for 2 h using a Live Cell Imaging System (Axio observer Z1, 10 \times , NA 0.55, Carl Zeiss, Germany). All the images were acquired at the same microscope settings in order to ensure reproducibility.

Intracellular uptake of MacTNP

MacTNP were diluted in the culture medium containing 10% FBS to obtain a final Ce6 concentration of 1 μM Ce6. Normal HDF cells were selected as ROS-negative control. HDF and Raw 264.7 cells were seeded in a 96-well plate at 1×10^4 cells/well and incubated for 24 h for cell attachment. Raw 264.7 cells were activated by treatment with LPS (1 $\mu\text{g}/\text{mL}$) and INF- γ (50 ng/mL) for 24 h. For comparison, both HDF cells and nonactivated macrophage cells were incubated for 24 h in the absence of LPS and INF- γ . Then the existing culture medium was replaced with 100 μL of fresh medium containing MacTNP. At 2 h post-incubation, all the cells were washed 3 times with PBS, and treated with 200 μL of 0.1 M NaOH/0.1% SDS solution for 2 h for inducing both cell lysis and complete disaggregation of the self-assembled MacTNP. Finally, the Ce6 fluorescence of the cell lysates was measured on a multifunctional microplate reader (λ_{ex} 400 nm, λ_{em} 660 nm). The fluorescence of MacTNP in the cell lysate was completely de-quenched by using 0.1 M NaOH/0.1% SDS, thereby enabling quantitative comparison of the internalized photosensitizers in the cells. As untreated controls, HDF, non-activated and activated macrophage cells were treated with cell culture media without MacTNP for 2 h. Then, the cells were washed 3 times with PBS, treated with 200 μL of 0.1 M

NaOH/0.1% SDS solution for 2 h, and the Ce6 fluorescence of the cell lysates was measured (λ_{ex} 400 nm, λ_{em} 660 nm). All the experiments were performed in quadruplicate.

Flow cytometric analysis and confocal fluorescence microscopy

To check the fluorescence recovery in macrophages, fluorescence intensities of the MacTNP-treated cells were measured by fluorescence-activated cell sorting (FACS). HDF and Raw 264.7 cells were plated at 1×10^6 cells/well onto a 12-well plate and incubated for 24 h for cell attachment. Raw 264.7 cells were activated with LPS (1 $\mu\text{g}/\text{mL}$) and INF- γ (50 ng/mL) for 24 h. For comparison, HDF and non-activated Raw 264.7 cells were incubated for 24 h in the absence of LPS and INF- γ . Then, the existing cell culture medium was replaced with fresh medium containing MacTNP at the equivalent concentration of 1 μM Ce6. After incubation for 2 h, the cells were washed 3 times with PBS, harvested, and their fluorescence intensities were analyzed by FACS (λ_{ex} 633 nm, λ_{em} 660 \pm 20 nm).

For NIR confocal fluorescence imaging study, Raw 264.7 cells were seeded at 1×10^5 cells/well in a LabTek II Chambered Coverglass (Nalge Nunc International Corp.) and incubated for 24 h for cell attachment. Activated macrophages were obtained by treating Raw 264.7 cells with LPS (1 $\mu\text{g}/\text{mL}$) and INF- γ (50 ng/mL) for 24 h. HDF and non-activated Raw 264.7 cells were incubated for 24 h in the absence of LPS and INF- γ . Then, the existing cell culture medium was replaced with fresh medium containing MacTNP (equiv. Ce6 concentration of 1 μM). After incubation for 2 h, the cells were washed 2 times with PBS, and incubated in fresh culture medium. NIR fluorescence images (λ_{ex} 633 nm, λ_{em} 700 \pm 50 nm) of the cells were acquired by confocal scanning-laser microscopy (CSLM, ZEISS LSM 510 META).

Cytotoxicity testing

Raw 264.7 macrophages were seeded in a 96-well plate at 1×10^4 cells/well, incubated for 24 h for cell attachment, and then activated with LPS and INF- γ for 24 h. MacTNP were diluted in cell culture medium containing 10% FBS to obtain Ce6 concentrations of 1 μM , 3 μM , 6 μM , and 10 μM , respectively. The existing culture medium was replaced with 100 μL of fresh medium containing MacTNP, and then the cells were further incubated for 24 h. After the cells were washed twice, fresh cell culture medium was added. The cell viability was measured using a cell counting kit (CCK-8; Dojindo Laboratories, Mashikimachi, Kumamoto, Japan). The absorbance was measured at 450 nm (reference = 650 nm) using a microplate reader

(Tecan Safire 2, Switzerland). The viability of the untreated controls was taken to be 100%, while the medium served as the background. Data are expressed as the mean (SD) of 4 data samples.

In vitro phototoxicity testing

Raw 264.7 macrophage cells were seeded in a 96-well plate at 1×10^4 cells/well, incubated for 24 h for cell attachment. Activated macrophages were obtained by treating Raw 264.7 cells with LPS (1 $\mu\text{g}/\text{mL}$) and INF- γ (50 ng/mL) for 24 h. HDF and non-activated Raw 264.7 cells were incubated for 24 h in the absence of LPS and INF- γ . Then, the existing cell culture medium was replaced with fresh medium containing MacTNP at the equivalent concentration of 1 μM Ce6. After incubation for 2 h, the cells were washed twice, fresh cell culture medium was added, and the cells were irradiated using a 670-nm CW laser at light doses of 5 and 10 J/cm² (light dose rate: 50 mW/cm²). The cells were further incubated for 18 h. The viability of the cells was analyzed using the CCK-8 kit. The viability of the untreated HDF and Raw 264.7 cell controls was taken to be 100%, while the medium served as the background. Data are ex-

pressed as the mean (SD) of 4 data samples.

Results and Discussion

Characterization of MacTNP

To synthesize HA-Ce6 conjugates, the carboxylic acids of the HA backbone were first modified with ethylene diamine and then conjugated with Ce6s using EDC/NHS chemistry (Figure 2 and Supplementary Material: Fig. S1). Based on the UV/Vis spectrum analysis, the number of conjugated Ce6s per a single HA backbone was calculated to be 91.

As expected, the amphiphilic HA-Ce6 conjugates self-assembled into nanoparticles having hydrodynamic size and zeta potential of 103.1 ± 38.4 nm and -22.6 ± 16.5 mV, respectively, in aqueous solution (Figure 3A). The significant broadening of the Soret band region in the UV/Vis spectrum of MacTNP (Figure 3B and Supplementary Material: Fig. S2) also confirmed the aggregation of the conjugated hydrophobic Ce6 molecules in the aqueous environment, while the negative zeta potential of the MacTNP indicated that the hydrophilic HA backbones were localized at the surface of MacTNP.

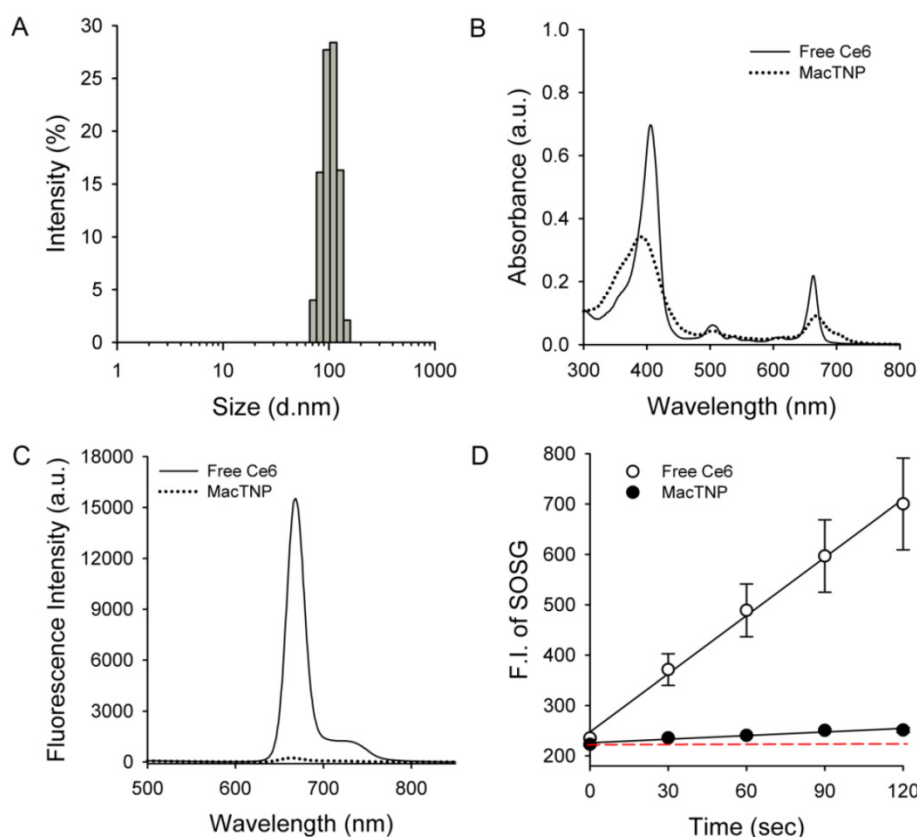


Fig 3. Characterization of MacTNP. (A) Hydrodynamic size distribution of MacTNP in PBS solution. (B) UV/Vis absorption and (C) fluorescence spectra of free Ce6 (solid line) and MacTNP (dotted line) at 5 μM Ce6. (D) Time-dependent singlet oxygen generation of free Ce6 and MacTNP during light irradiation (670-nm CW laser, light dose rate: 50 mW/cm²). The dashed line represents the baseline SOSG fluorescence.

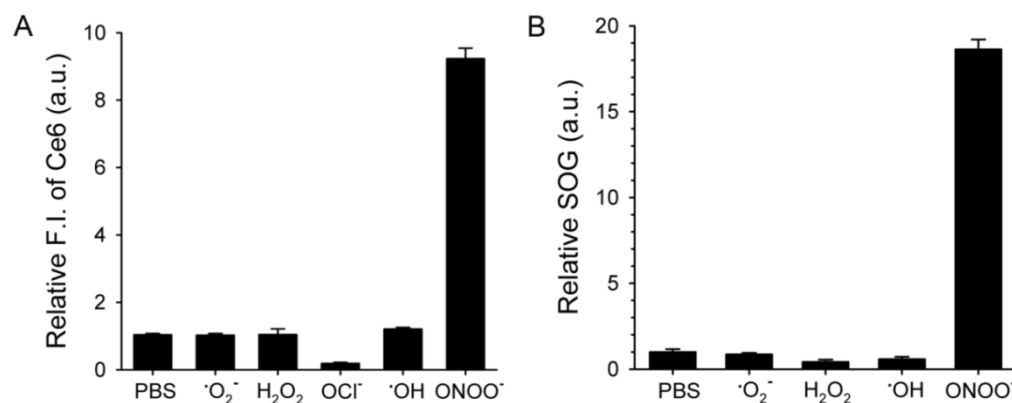


Fig 4. ROS-responsive recovery of fluorescence and SOG. MacTNPs were reacted with various ROS (n=4). Then, (A) the Ce6 fluorescence in the samples was measured and compared with that of the control (i.e., PBS-treated MacTNP). (B) Relative SOG after treatment with ROS. ROS-treated samples were irradiated using a 670-nm CW laser for 120 s, and the relative SOG was calculated by comparing the normalized SOSG fluorescence of the samples with that of the control.

As shown in Figure 3C, due to the aggregation of Ce6s in the self-assembled nanoparticles, the fluorescence of MacTNP was dramatically quenched (i.e., only 1.6% of the fluorescence intensity of free Ce6). A consistent quenching in the MacTNP production of reactive singlet oxygen was observed, where the singlet oxygen sensor green (SOSG) reagent was used as a probe to detect SOG by free Ce6 and MacTNP (Figure 3D). During the 670-nm laser irradiation, in comparison to that from free Ce6, a minor increase in the SOSG fluorescence emission was observed for MacTNP, indicating that MacTNP SOG was inhibited. SOG from MacTNP was 16-fold lower than that from free Ce6.

ROS-responsive recovery of fluorescence and SOG in the MacTNP

Next, we checked if ROS could act as a switch for fluorescence emission recovery and SOG by de-quenching of Ce6 by degrading MacTNP (Figure 4). Previous studies have examined the degradation of HA backbones and its mechanism [38-41]. In particular, peroxynitrite is known to induce HA fragmentation in a site-selective manner at the *N*-acetylglucosamine β -(1 \rightarrow 4) glycosidic bonds resulting in the formation of oligosaccharides differing by disaccharide units [39]. Accordingly, we expected that the degradation of MacTNP upon ROS treatment would result in the release of Ce6 and the subsequent recovery of the fluorescence intensity. When MacTNP in PBS (0.5 μM Ce6) were treated with various chemically generated ROS at 50 μM for 2 h, only peroxynitrite (ONOO $^-$)-treated MacTNP showed 9.3-fold increase in the fluorescence intensity compared to PBS-treated MacTNP as the control (Figure 4A). The other ROS did not induce a significant recovery of MacTNP fluorescence, probably because of insufficient disintegration of the self-assembled MacTNP.

When fluorescence intensity of MacTNP incubated with peroxynitrite at different concentrations (0, 5, 10, 20, 40, and 100 μM) was measured, fluorescence recovery of MacTNP was dose-dependent on the peroxynitrite concentration (Supplementary Material: Figure S3). Particularly, there was a linear dependence ($r^2 = 0.959$) of the fluorescence intensity on the peroxynitrite concentration in the 0 – 40 μM range. Previous reports note that the stimulated expression of inducible nitric oxide synthase is associated with atherosclerosis, and the activity of this enzyme preferentially promotes the formation of peroxynitrite [42]. Therefore, the dose-dependent fluorescence recovery of MacTNP by peroxynitrite suggests that MacTNP may also be useful for the specific imaging of peroxynitrite levels in atherosclerotic lesions.

Before examining SOG recovery, we checked whether ROS caused any change in the fluorescence intensity of SOSG reagent. Since NaOCl caused the denaturation of Ce6 (Supplementary Material: Figure S4), we excluded the NaOCl-treated samples in this experiment. As a result, it was confirmed that ROS did not affect SOSG fluorescence (Supplementary Material: Figure S5). As in the fluorescence experiment, the treatment of MacTNP with peroxynitrite induced an 18-fold increase in SOG while the other ROS produced no significant increases (Figure 4B).

Effect of HAdase on the fluorescence recovery of MacTNP

HAdase rapidly degrades HA through preferential cleavage of β -(1 \rightarrow 4) glycosidic bonds [43], similar to peroxynitrite. HAdase activity has been reported to increase in atheromatous plaques [44]. Therefore, we checked if MacTNP fluorescence could be affected by HAdase in addition to ROS (Figure 5). Interestingly, the effect of HAdase on the fluorescence intensity of MacTNP was negligible, showing only 30% increase

in MacTNP fluorescence even upon treatment with 100 U/mL HAase.

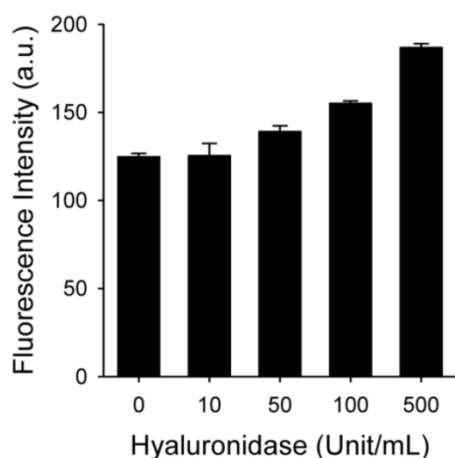


Fig 5. Fluorescence intensity of MacTNP after treatment with different concentrations of hyaluronidase (n=4).

Live cell imaging of fluorescence recovery in activated macrophage cells

In order to demonstrate the utility of MacTNP in macrophage-targeted imaging, we applied both free Ce6 and MacTNP to the activated Raw 264.7 cells (Figure 6). Since the fluorescence of MacTNP is expected to be quenched in the extracellular environment and turned on only inside the activated macrophages, the NIR fluorescence were acquired every 15 min for 2 h without washing the photosensitizers. As expected, only weak fluorescent signals were detected in the extracellular space surrounding the MacTNP-treated cells at 15 min, whereas a highly intense fluorescence was continuously observed in the free Ce6-treated cells. As shown in Figure 6 (upper images), the cells became noticeably brighter with time and were strongly fluorescent after 2 h of incubation, indicating the fluorescence turn-on inside the cells. This result indicates that activatable MacTNP are potentially useful in the selective NIR fluorescence imaging of atherosclerotic lesions with a high target-to-background ratio *in vivo*.

Intracellular uptake of MacTNP in normal fibroblast and macrophage cells

Before evaluating differences in fluorescence activation of MacTNP in normal HDF and macrophage cells, we compared the amount of MacTNP intracellular uptake in these cells. HDF, non-activated and activated Raw 264.7 cells were incubated with MacTNP at Ce6 concentration of 1 μ M for 2 h, washed 3 times with PBS, treated with 0.1 M NaOH/0.1% SDS solution for inducing both cell lysis and disaggregation of the self-assembled MacTNP, and fluorescence

intensities of the cell lysates were measured. Since treatment of the cells with 0.1 M NaOH/0.1% SDS solution induces complete disassembly of MacTNP and subsequent de-quenching of Ce6 fluorescence, intracellular uptake of MacTNP in these cells could be compared by measuring fluorescence intensities of Ce6 in the cell lysates. Strong NIR fluorescence was measured from the MacTNP-treated cells while minor fluorescence was detected from the untreated control cells (Figure 7A). There was no statistically significant difference in fluorescence intensity between the cells, indicating that similar amount of MacTNP was internalized.

Flow cytometric analysis and confocal fluorescence microscopy

Recovery of Ce6 fluorescence in the activated macrophages was further evaluated by FACS analysis (Figure 7B). HDF, non-activated and activated Raw 264.7 cells were incubated with MacTNP at Ce6 concentration of 1 μ M for 2 h, washed 3 times with PBS, harvested, and their fluorescence intensities analyzed by FACS. MacTNP-treated activated Raw 264.7 cells showed 3-fold greater mean fluorescence intensity than MacTNP-treated HDF cells. Also mean fluorescence intensity of the MacTNP-treated non-activated Raw 264.7 cells was only 61% of that of the MacTNP-treated activated Raw 264.7 cells. Since intracellular uptake of MacTNP was similar in these cells (Figure 7A), FACS results indicate the release of Ce6 molecules from MacTNP, with subsequent fluorescence recovery inside the activated macrophage cells. In addition, significantly higher fluorescence recovery of MacTNP was obtained in the activated macrophages compared to their non-activated counterparts. NIR fluorescence images obtained by confocal laser scanning microscopy (CLSM) also supported MacTNP fluorescence recovery within the activated Raw 264.7 cells (Figure 7C).

Cytotoxicity testing

Activated Raw 264.7 cells were treated with MacTNP for 24 h over a Ce6 concentration range of 0–10 μ M in order to determine Ce6 toxicity in the dark. As expected, cells treated with MacTNPs showed no cytotoxicity even at the highest Ce6 concentration (Figure 8A), confirming the excellent biocompatibility of MacTNP.

In vitro phototoxicity testing

In contrast to the dark cytotoxicity test, cell viability following treatment with MacTNP (equiv. Ce6 concentration of 1 μ M) decreased in a light dose-dependent manner upon irradiation with 670-nm CW laser (Figure 8B). In particular, 66% of the

activated Raw 264.7 cells were dead after light irradiation (10 J/cm²) whereas no statistically significant decrease in cell viability was observed in the HDF cells after light irradiation. As expected from the FACS analysis, PDT effect of MacTNP in the activated

macrophages was significantly higher than in non-activated macrophage cells ($P < 0.001$). The order of phototoxicity observed was HDF < non-activated Raw 264.7 cells < activated Raw 264.7 cells.

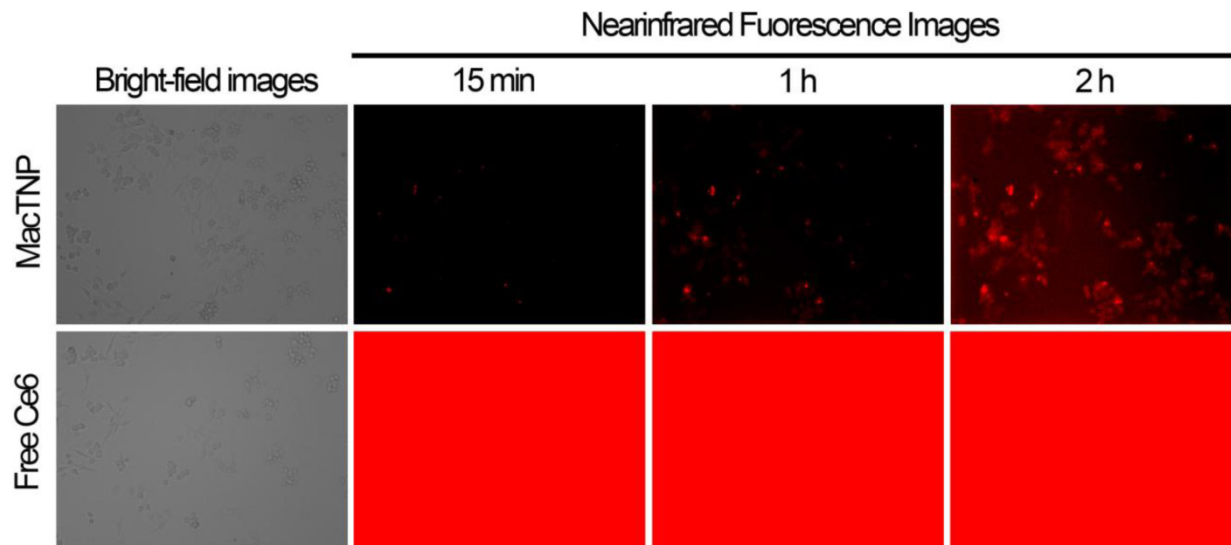


Fig 6. NIR fluorescence images obtained from live cell fluorescence microscopy. Activated macrophages were incubated with MacTNP and free Ce6 at 1 μ M Ce6, and then, without washing the cells, NIR fluorescence images were obtained every 15 min for 2 h. The red color indicates the fluorescence signals generated from Ce6 photosensitizers (λ_{ex} 640 \pm 15 nm, λ_{em} 690 \pm 25 nm).

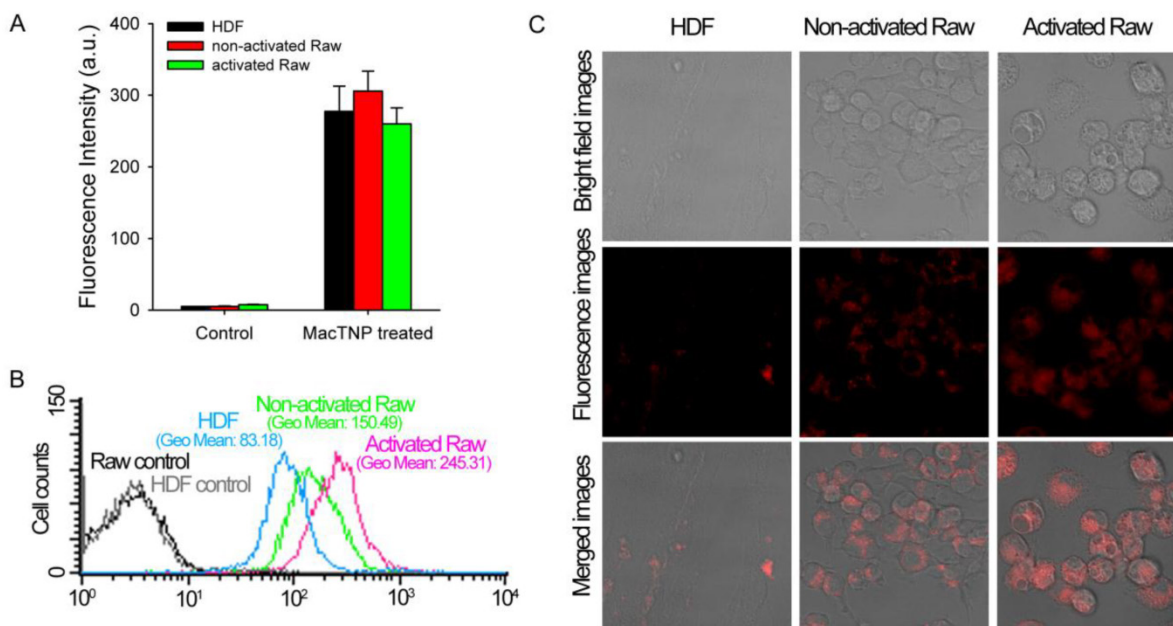


Fig 7. (A) Fluorescence intensities measured from the cell lysates (λ_{ex} 400 nm, λ_{em} 660 nm). MacTNPs in the cell lysates were completely de-quenched by 0.1 M NaOH/0.1% SDS solution, thereby enabling comparison of the amount of photosensitizer in the cell lysates. No significant difference in Ce6 fluorescence was observed between MacTNP-treated cells ($n = 4$). (B) Flow cytometric analysis of Ce6 fluorescence in HDF, non-activated and activated Raw 264.7 cells (λ_{ex} 633 nm, λ_{em} 660 \pm 20 nm). (C) Confocal scanning fluorescence images of the MacTNP-treated HDF, non-activated and activated macrophages (λ_{ex} 633 nm, λ_{em} 700 \pm 50 nm).

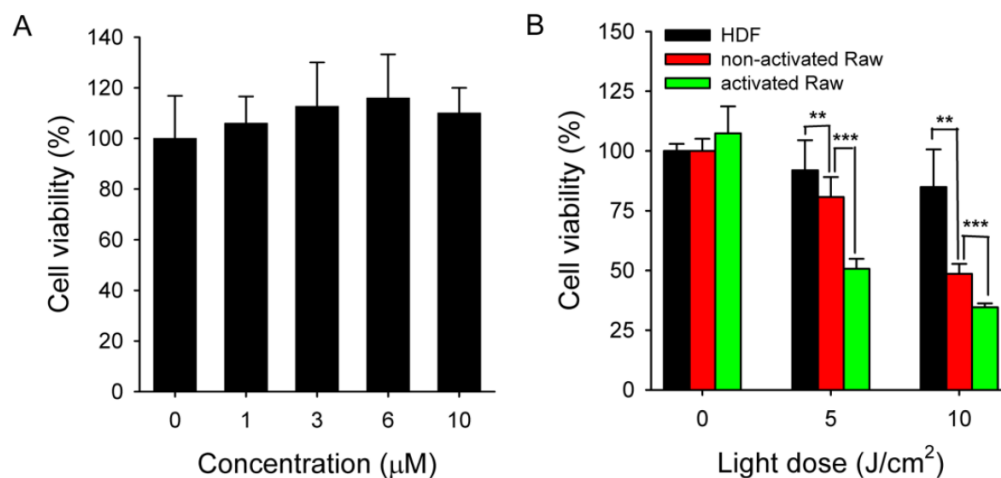


Fig 8. (A) Dark toxicity testing of MacTNP. Cells were treated with MacTNPs at various concentrations for 24 h and cell viability was measured without light irradiation ($n = 4$). (B) *In vitro* phototoxicity test ($n = 4$). Cells were treated with MacTNP at Ce6 concentration of 1 µM for 2 h, washed 2 times, and irradiated using a 670-nm CW laser at various light doses (light dose rate: 50 mW/cm²). ** $P < 0.01$, *** $P < 0.001$.

Conclusions

Biocompatible MacTNP are nonfluorescent and nonphototoxic in their native state. However, they become highly fluorescent and phototoxic upon treatment with peroxyxynitrite. *In vitro* cell studies confirm that the fluorescence emission and SOG of MacTNP are recovered inside the activated macrophages. We believe that the MacTNPs developed in this study may be potentially useful for selective NIR fluorescence imaging and PDT of atherosclerosis lesions *in vivo*.

Supplementary Material

Fig.S1 - Fig.S5.

<http://www.thno.org/v04p0001s1.pdf>

Acknowledgements

This work was supported by a National Cancer Center grant (1310160-1) and the Pioneer Research Center Program of Korea funded by the Ministry of Science, ICT & Future Planning (2013-009119), Republic of Korea.

Conflict of Interests

The authors have declared that no competing interest exists.

References

- Farb A, Burke AP, Tang AL, Liang TY, Mannan P, Smialek J, Virmani R. Coronary plaque erosion without rupture into a lipid core: a frequent cause of coronary thrombosis in sudden coronary death. *Circulation* 1996; 93: 1354-63.
- Virmani R, Kolodgie F, Burke A, Farb A, Schwartz SM. Lessons from sudden coronary death: a comprehensive morphological classification scheme for atherosclerotic lesions. *Arterioscler Thromb Vasc Biol* 2000; 20: 1262-75.
- Hellings WE, Peeters W, Moll FL, Pasterkamp G. From vulnerable plaque to vulnerable patient: the search for biomarkers of plaque destabilization. *Trends Cardiovasc Med* 2007; 17: 162-71.
- Cassells W, Hathorn B, David M, Krabach T, Vaughn WK, McAllister HA, Bearman G, Willerson JT. Thermal detection of cellular infiltrates in living

- atherosclerotic plaques: possible implications for plaque rupture and thrombosis. *Lancet* 1996; 347: 1447-51.
- Amirbekian V, Lipinski MJ, Briley-Saebo KC, Amirbekian S, Aguinaldo JGS, Weinreb DB, Vucic E, Frias JC, Hyafil F, Mani V, Fisher EA, Fayad ZA. Detecting and assessing macrophages in vivo to evaluate atherosclerosis noninvasively using molecular MRI. *Proc Natl Acad Sci USA* 2007; 104: 961-6.
- Jaffer FA, Libby P, Weissleder R. Molecular imaging of cardiovascular disease. *Circulation* 2007; 116: 1052-61.
- McCarthy JR. Nanomedicine and cardiovascular disease. *Curr Cardiovasc Imaging Rep* 2010; 3: 42-9.
- Dolmans DE, Dai Fukumura RKJ. Photodynamic therapy of cancer. *Nat Rev Cancer* 2003; 3: 380-7.
- Waksman R, McEwan PE, Moore TI, Pakala R, Kologdie FD, Hellings DG, Seabron RC, Rychnovsky SJ, Vasek J, Scott RW, Virmani R. PhotoPoint photodynamic therapy promotes stabilization of atherosclerotic plaques and inhibits plaque progression. *J Am Coll Cardiol* 2008; 52: 1024-32.
- Peng C, Li Y, Liang H, Cheng J, Li Q, Sun X, Li Z, Wang F, Guo Y, Tian Z, Yang L, Tian Y, Zhang Z, Cao W. Detection and photodynamic therapy of inflamed atherosclerotic plaques in the carotid artery of rabbits. *J Photochem Photobiol B* 2011; 102: 26-31.
- Kossodo S, LaMuraglia GM. Kossodo S, LaMuraglia GM. Clinical potential of photodynamic therapy in cardiovascular disorders. *Am J Cardiovasc Drugs* 2001; 1: 15-21.
- Hsiang Y, Stonefield M, Bower RD, Fragoso M, Tsang V, Crespo MT, Lundkvist A. Assessing Photofrin uptake in atherosclerosis with a fluorescent probe: comparison with photography and tissue measurements. *Lasers Surg Med* 1993; 13: 271-8.
- Hsiang YN, Crespo MT, Richter AM, Jain AK, Fragoso M, Levy JG. In vitro and in vivo uptake of benzoporphyrin derivative into human and miniswine atherosclerotic plaque. *Photochem Photobiol* 1993; 57: 670-4.
- Litvack F, Grundfest WS, Forrester JS, Fishbein MC, Swan HJ, Corday E, Rider DM, McDermid IS, Pacala TJ, Laudenslager JB. Effects of hematoporphyrin derivative and photodynamic therapy on atherosclerotic rabbits. *Am J Cardiol* 1985; 56: 667-71.
- Kereiakes DJ, Szymszewska AM, Wahr D, Herrmann HC, Simon DL, Rogers C, Kramer P, Shear W, Yeung AC, Shunk KA, Chou TM, Popma J, Fitzgerald P, Carroll TE, Forer D, Adelman DC. Phase I drug and light dose-escalation trial of motexafin lutetium and far red light activation (phototherapy) in subjects with coronary artery disease undergoing percutaneous coronary intervention and stent deployment: procedural and long-term results. *Circulation* 2003; 108: 1310-5.
- Liu Q, Hamblin MR. Macrophage-targeted photodynamic therapy: Scavenger receptor expression and activation state. *Int J Immunopathol Pharmacol* 2005; 18: 391-402.
- McCarthy JR, Jaffer FA, Weissleder R. A macrophage-targeted theranostic nanoparticle for biomedical applications. *Small* 2006; 2: 983-7.
- Tawakol A, Castano AP, Anetelli F, Bashian G, Stern J, Zahra T, Gad F, Chirico S, Ahmadi A, Fischman AJ, Muller JE, Hamblin MR. Photosensitizer delivery to vulnerable atherosclerotic plaque: comparison of macrophage-targeted conjugate versus free chlorin(e6). *J Biomed Opt* 2006; 11: 021008.
- Kamat M, El-Boubbou K, Zhu DC, Lansdell T, Lu X, Li W, Huang X. Hyaluronic acid immobilized magnetic nanoparticles for active targeting and imaging of macrophages. *Bioconjug Chem* 2010; 21: 2128-35.
- McCarthy JR, Korngold E, Weissleder R, Jaffer FA. A light-activated theranostic nanoagent for targeted macrophage ablation in inflammatory atherosclerosis. *Small* 2010; 6: 2041-49.

21. Lovell JK, Liu TW, Chen J, Zheng G. Activatable photosensitizers for imaging and therapy. *Chem Rev* 2010; 110: 2839-57.
22. Choi Y, Weissleder R, Tung CH. Selective antitumor effect of novel protease-mediated photodynamic agent. *Cancer Res* 2006; 66: 7225-9.
23. Jang B, Park JY, Tung CH, Kim IH, Choi Y. Gold nanorod-photosensitizer complex for near-infrared fluorescence imaging and photodynamic/photothermal therapy in vivo. *ACS Nano* 2011; 5: 1086-94.
24. Bae BC, Na K. Self-quenching polysaccharide-based nanogels of pullulan/folate-photosensitizer conjugates for photodynamic therapy. *Biomaterials* 2010; 31: 6325-35.
25. Park W, Park SJ, Na K. The controlled photoactivity of nanoparticles derived from ionic interactions between a water soluble polymeric photosensitizer and polysaccharide quencher. *Biomaterials* 2011; 32: 8261-70.
26. Park SY, Baik HJ, Oh YT, Oh KT, Youn YS, Lee ES. A smart polysaccharide/drug conjugate for photodynamic therapy. *Angew Chem Int Ed* 2011; 50: 1644-7.
27. Yoon HY, Koo H, Choi KY, Lee SJ, Kim K, Kwon IC, Leary JF, Park K, Yuk SH, Park JH, Choi K. Tumor-targeting hyaluronic acid nanoparticles for photodynamic imaging and therapy. *Biomaterials* 2012; 33: 3980-9.
28. Jang B, Choi Y. Photosensitizer-conjugated gold nanorods for enzyme-activatable fluorescence imaging and photodynamic therapy. *Theranostics* 2012; 2: 190-7.
29. Cho Y, Choi Y. Graphene oxide-photosensitizer conjugate as a redox-responsive theranostic agent. *Chem Commun* 2012; 48: 9912-4.
30. Cho Y, Kim H, Choi Y. A graphene oxide-photosensitizer complex as an enzyme-activatable theranostic agent. *Chem Commun* 2013; 49: 1202-4.
31. Shon SM, Choi Y, Kim JY, Lee DK, Park JY, Schellingerhout D, Kim DE. Photodynamic therapy using a protease-mediated theranostic agent reduces cathepsin-B activity in mouse atheromata in vivo. *Arterioscler Thromb Vasc Biol* 2013; 33: 1360-5.
32. Bogdan C, Rollinghoff M, Diefenbach A. Reactive oxygen and reactive nitrogen intermediates in innate and specific immunity. *Curr Opin Immunol* 2000; 12: 64-76.
33. Kohr MJ, Roof SR, Zweier JL, Ziolo MT. Modulation of myocardial contraction by peroxynitrite. *Front Physiol* 2012; 3: 468.
34. Pennathur S, Bergt C, Shao B, Byun J, Kassim SY, Singh P, Green PS, McDonald TO, Brunzell J, Chait A, Oram JF, O'Brien K, Geary RL, Heinecke JW. Human atherosclerotic intima and blood of patients with established coronary artery disease contain high density lipoprotein damaged by reactive nitrogen species. *J Biol Chem* 2004; 279: 42977-83.
35. Duan J, Kasper DL. Oxidative depolymerization of polysaccharides by reactive oxygen/nitrogen species. *Glycobiology* 2011; 21: 401-9.
36. Lee H, Lee K, Kim IK, Park TG. Fluorescent gold nanoprobe sensitive to intracellular reactive oxygen species. *Adv Funct Mater* 2009; 19: 1884-90.
37. Hamblin MR, Miller JL, Rizvi I. Pegylation of a chlorin(e6) polymer conjugate increases tumor targeting of photosensitizer. *Cancer Res* 2001; 61: 7155-62.
38. Soltes L, Mendichi R, Kogan G, Schiller J, Stankovska M, Amhold J. Degradative action of reactive oxygen species on hyaluronan. *Biomacromolecules* 2006; 7: 659-68.
39. Kennett EC, Davies MJ. Degradation of matrix glycosaminoglycans by peroxynitrite/peroxynitrous acid: Evidence for a hydroxyl-radical-like mechanism. *Free Radic Biol Med* 2007; 42: 1278-89.
40. Li M, Rosenfeld L, Vilar RE, Cowman MK. Degradation of Hyaluronan by Peroxynitrite. *Arch Biochem Biophys* 1997; 341: 245-50.
41. Corsaro MM, Pietraforte D, Di Lorenzo AS, Minetti M, Marino G. Reaction of peroxynitrite with hyaluronan and related saccharides. *Free Radic Res* 2004; 38: 343-53.
42. Buttery LD, Sqringall DR, Chester AH, Evans TJ, Standfield EN, Parums DV, Yacoub MH, Polak JM. Inducible nitric oxide synthase is present within human atherosclerotic lesions and promotes the formation and activity of peroxynitrite. *Lab Invest* 1996; 75: 77-85.
43. Girish KS, Kemparaju K. The magic glue hyaluronan and its eraser hyaluronidase: a biological overview. *Life Sci* 2007; 80: 1921-43.
44. Bot PT, Pasterkamp G, Goumans MJ, Strijder C, Moll FL, de Vries JP, Pals ST, de Kleijn DP, Piek JJ, Hofer IE. Hyaluronic acid metabolism is increased in unstable plaques. *Eur J Clin Invest* 2010; 40: 818-27.